Int. J. Electrochem. Sci., 14 **(2019)** 10375 – 10386, doi: 10.20964/2019.11.32

International Journal of
ELECTROCHEMICAL
SCIENCE
www.electrochemsci.org

Excellent cycling performance of $LiMn_{1.92}Al_{0.04}Si_{0.04}O_4$ nanorods as cathode material for lithium-ion battery

Hongyuan Zhao[*], *Li Dong, Mingming Zhang, Yaqi Zhang, Tingting Wu, Yongfeng Li* [*]

Henan Institute of Science and Technology, Xinxiang 453003, China
[*]E-mail: hongyuanzhao@126.com (H. Zhao); lyf16816800@163.com (Y. Li)

Received: 23 June 2019 / *Accepted:* 19 August 2019 / *Published:* 7 October 2019

For the purpose of enhancing the cycling performance of $LiMn_2O_4$, the strategy of synergistic modification has been developed based on the simultaneous employment of the Al-Si co-doping and nano-rod micrograph. In addition, the preparation of $LiMn_{1.92}Al_{0.04}Si_{0.04}O_4$ nanorods can be conducted by a simple and low-cost two-step method due to hydrothermal reaction and subsequent process of lithiation. The Al-Si co-doping has positive effect on inhibiting the distortion effect of Jahn-Teller and strengthening the structural stability, and the nano-sized rod-like micrograph can further enhance the electrical conductivity. The results obtained from electrochemical test show that the comprehensive usage of Al-Si co-doping and nano-sized rod-like micrograph demonstrates the synergistic effect. In comparison with the undoped $LiMn_2O_4$ and $LiMn_{1.92}Al_{0.04}Si_{0.04}O_4$ particles, the $LiMn_{1.92}Al_{0.04}Si_{0.04}O_4$ nanorods are able to show more excellent cycling performance and it can present higher capacity retention of 97.1% after 100 cycles when tested at 1.0 C. Especially, the $LiMn_{1.92}Al_{0.04}Si_{0.04}O_4$ nanorods can deliver a satisfactory reversible capacity of 95.1 mAh g^{-1} with capacity retention of 89.3% after 100 cycles at 5.0 C under the circumstances of high temperature. It is shown by such excellent performance that the strategy of synergistic modification based on the simultaneous usage of the Al-Si co-doping and nano-rod micrograph is of great significance to developing the lithium manganate-based cathode material of high performance.

Keywords: $LiMn_2O_4$; Al-Si co-doping; Nano-rod micrograph; Synergistic effect; Cycling performance

1. INTRODUCTION

Nowadays, it is widely acknowledged that lithium ion batteries are of great significance to promoting the industry of new-energy vehicles [1-3]. In comparison with other commercial cathode materials, the spinel lithium manganese oxides ($LiMn_2O_4$) is known for its high performance-price-ratio due to the abundant manganese resource used, the unique character of environmental friendliness, and the mature technology employed in preparation [4-7]. However, what is somewhat regrettable is the problem that the poor cycling performance severely restricts the large-scale application of $LiMn_2O_4$. It

can be easily obtained from the existing literatures [8-12] that the Jahn-Teller distortion effect of Mn^{3+} ions and Mn dissolution is able to impose significant negative effect on the electrochemical performance.

In order to improve the electrochemical performance, scientific researchers have carried out intensive research works in large amount and developed many valuable strategies for modification, such as the optimization of synthesis technology, doping and surface coating [13-18]. Among these strategies, the surface coating is recognized for making full use of the coating layer so as to avoid the direct contact of active material and the electrolyte [11, 19]. As a consequence, the dissolution of manganese can be effectively restrained and the cycling performance can be greatly promoted. However, it is of great significance to note that the surface coating is unable to deal with the problem, the inherent instability of $LiMn_2O_4$, effectively. In contrast, the doping strategy can make great contribution to the improvement of the structural stability by replacing partial manganese ions with other ions such as Mg^{2+}, Cu^{2+}, Zn^{2+}, Ni^{3+}, Co^{3+}, Al^{3+}, Ti^{4+}, Si^{4+}, etc [3,9,20-26]. These heterogeneous ions mentioned above can play quite significant role in inhibiting the Jahn-Teller distortion effect and strengthening the spinel structure. Among these ions mentioned above, the aluminum ions have quite excellent effect on improving the cycling stability. Guo et al. [27] have ever reported the inhibiting effect imposed by Al-doping on the Jahn-Teller distortion effect. It is known that the Al-doping is also able to reduce the lattice parameters and then enable the distribution of particle size to be more uniform. However, it should also be noted that the addition of aluminium ions would result in the reduction of trivalent manganese ions, which would consequently decrease the reversible capacity of $LiMn_2O_4$ [8, 28]. Based on our works carried out previously [24, 29], the Si-doping can make up for the shortage of the low-valent ions-doping with regard to the discharge capacity. In addition [26], we have found previously that the Si-doping has a positive function in increasing the reversible capacity of the Mg-doped $LiMn_2O_4$. Therefore, it is reasonable to enhance the comprehensive performance if Al-doping and Si-doping are used simultaneously. Apart from that, the nanostructured morphologies is able to impose a positive effect on the reversible capacity and cycling stability [30, 31]. Especially, the nano-sized rod-like micrograph are able to make the best use of one-dimensional electron transport pathway for the purpose of enhancing the electronic conductivity [32]. Above all, it is novel and interesting to use the collaboration strategy based on the Al-Si co-doping and nano-sized rod-like micrograph for the purpose of achieving optimal performance of $LiMn_2O_4$.

It is also known that there is no report on this synergistic modification scheme. In this work, the preparation of $LiMn_{1.92}Al_{0.04}Si_{0.04}O_4$ nanorods were carried out through the employment of a simple and low-cost two-step method on account of hydrothermal reaction and subsequent lithiation process. More than that, the investigation on the synergistic effects of Al-Si co-doping and nano-sized rod-like micrograph on the structure, morphology and electrochemical properties of $LiMn_2O_4$ were conducted in detail.

2. EXPERIMENTAL

In terms of the $LiMn_{1.92}Al_{0.04}Si_{0.04}O_4$ nanorods, they were prepared through the employment of a simple and low-cost two-step method on account of hydrothermal reaction and subsequent lithiation

process. With regard to aluminum nitrate, tetraethoxysilane (TEOS), and self-synthesized γ-MnOOH nanorods, they are applied as doping agent and manganese source, respectively. At the initial stage, the γ-MnOOH nanorods were obtained by using the hydrothermal method according to the work carried out previous [32]. In order to prepare the $LiMn_{1.92}Al_{0.04}Si_{0.04}O_4$ nanorods, $LiOH{\cdot}H_2O$, γ-MnOOH, $Al(NO_3)_3{\cdot}9H_2O$, and $C_8H_{20}O_4Si$ were ground under the assistance of absolute ethanol, which was followed by drying the slurry mixture obtained in vacuum drying oven. After that, the homogeneous mixture was sintered at the temperature of 700 °C for 10 h in muffle furnace. For the purpose of comparison, the undoped $LiMn_2O_4$ and $LiMn_{1.92}Al_{0.04}Si_{0.04}O_4$ particles were prepared by solid-state reaction process with electrolytic MnO_2 as manganese precursor.

The analysis was carried out for both the structures and morphologies of all these samples obtained through the employment of X-ray powder diffraction (XRD) and scanning electron microscopy (SEM). Then, with regard to the composition and element distribution, they were explored by adopting XPS pattern, EDS analysis and SEM mapping images. After that, the studies on the effects imposed by Al-Si co-doping and nano-sized rod-like micrograph on the electrochemical performance of $LiMn_2O_4$ were carried out by employing the LAND battery testing system and CHI660E electrochemical workstation.

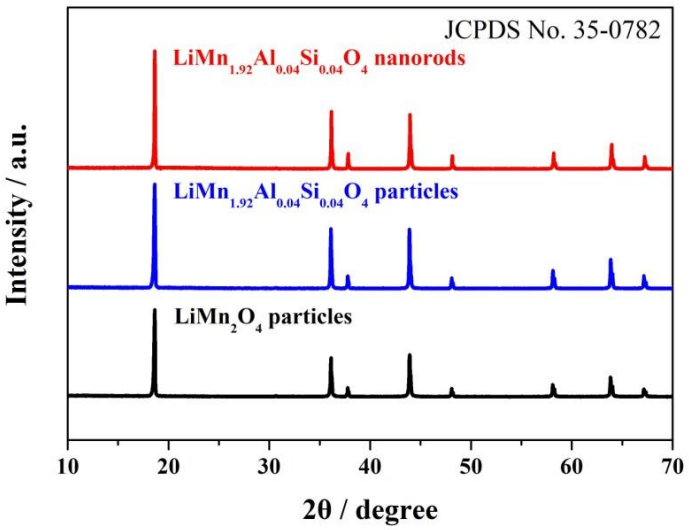

Figure 1. XRD patterns of the $LiMn_2O_4$ particles, $LiMn_{1.92}Al_{0.04}Si_{0.04}O_4$ particles and $LiMn_{1.92}Al_{0.04}Si_{0.04}O_4$ nanorods.

3. RESULTS AND DISCUSSION

In order to remove the effect imposed by the Al-Si co-doping and nano-sized rod-like micrograph on the structure of $LiMn_2O_4$, the technique of X-ray diffraction was conducted so as to study the $LiMn_2O_4$ particles, $LiMn_{1.92}Al_{0.04}Si_{0.04}O_4$ particles and $LiMn_{1.92}Al_{0.04}Si_{0.04}O_4$ nanorods. **Fig. 1** shows corresponding results obtained from XRD. It is shown by the figure that the undoped $LiMn_2O_4$ particles

demonstrate obvious diffraction peaks, which are indexed to $LiMn_2O_4$ (JCPDS No. 35-0782). However, no diffraction peaks are available for the manganese oxides, which suggests that the $LiMn_2O_4$ sample obtained possesses high purity [32]. With regard to the Al-Si co-doped $LiMn_2O_4$ samples, it can be observed that the introduction of aluminum and silicon ions is unable to change the phase structure of $LiMn_2O_4$. In addition, all the peaks for characteristic diffraction are almost in total agreement with that of $LiMn_2O_4$ and these peaks are stronger in comparison with that of the undoped $LiMn_2O_4$ particles. Especially, the $LiMn_{1.92}Al_{0.04}Si_{0.04}O_4$ nanorods show the strongest and sharpest diffraction peaks, which as a consequence indicate the good quality of crystalline.

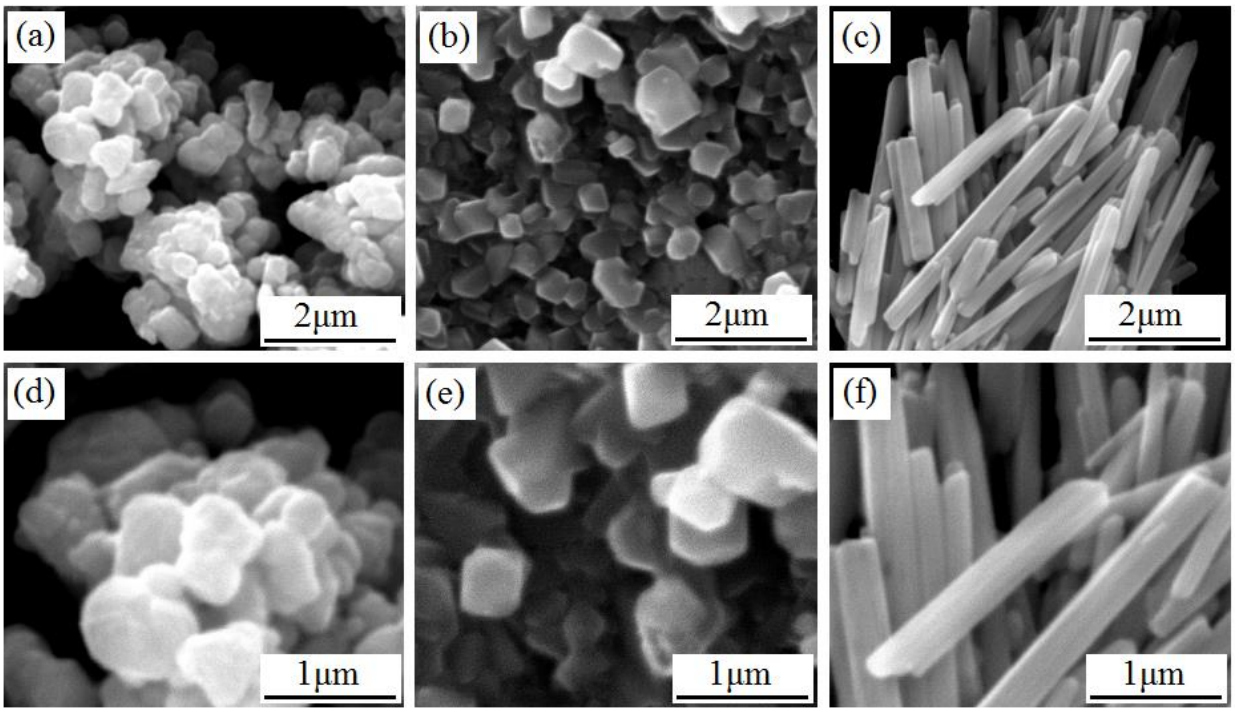

Figure 2. SEM images of the $LiMn_2O_4$ particles (a, d), $LiMn_{1.92}Al_{0.04}Si_{0.04}O_4$ particles (b, e), and $LiMn_{1.92}Al_{0.04}Si_{0.04}O_4$ nanorods (c, f).

Fig. 2 shows the SEM images of the $LiMn_2O_4$ particles, $LiMn_{1.92}Al_{0.04}Si_{0.04}O_4$ particles and $LiMn_{1.92}Al_{0.04}Si_{0.04}O_4$ nanorods, from which it can be observed obviously that completely different micro-morphologies are shown by these two samples. As shown in **Fig. 2a** and **d**, the undoped $LiMn_2O_4$ particles show irregular morphology of particle with non-uniform distribution of particle size, and a certain degree of agglomeration is also available. It is then suggested by this unsatisfactory fact that it is quite difficult for the undoped $LiMn_2O_4$ particles to show good electrochemical properties [34]. In sharp contrast, the $LiMn_{1.92}Al_{0.04}Si_{0.04}O_4$ particles (**Fig. 2b** and **e**) show relatively uniform size distribution of particle, indicating that the Al-Si co-doping is able to exert positive available action in inhibiting the agglomeration of particles. As for the $LiMn_{1.92}Al_{0.04}Si_{0.04}O_4$ nanorods (**Fig. 2c** and **f**), it is easy for us to observe that this material presents obvious rod-shaped morphology, which further shows that the nano-rod micrograph of manganese source is well maintained in the process of Al-Si coped $LiMn_2O_4$ nanorods.

Both the EDS method and SEM Mapping technology are adopted in order to explore the

composition and element distribution, as shown in **Fig. 3**. **Fig. 3b** shows that the EDS pattern presents the existence of Mn, Al, Si, O elements in the $LiMn_{1.92}Al_{0.04}Si_{0.04}O_4$ nanorods. What should be focused on is that the appearance of Au element is attributed to the gold sputtering pretreatment before the SEM analysis. Moreover, it can be seen that the elements of Mn, Al, Si, O are all evenly distributed in the Al-Si co-doped $LiMn_2O_4$ product with nano-rod morphology. On the basis of the reported works [35, 36], it is easy to come to the conclusion that the XPS technology plays a significant role in analyzing the composition and chemical state of each element. **Fig. 4** shows the XPS spectra of the $LiMn_{1.92}Al_{0.04}Si_{0.04}O_4$ nanorods. It has been reported that the binding energy peaks of $Mn2p_{3/2}$ include Mn^{3+} and Mn^{4+} ions, and they are actually located at 641.8 eV and 643.3 eV, respectively [33]. As a matter of fact, the binding energy peak of $Mn2p_{3/2}$ shown in **Fig. 4b** is located at 642.3 eV, which suggests the mixed state of Mn^{3+} and Mn^{4+} in the $LiMn_{1.92}Al_{0.04}Si_{0.04}O_4$ nanorods. In terms of the Al2p and Si2p elements, the peaks of binding energy shown in **Fig. 4c** and **d** are located at 74.2 and102.7 eV which are assigned to Al^{3+} and Si^{4+}, respectively, which are in agreement with the results obtained previously [33,34].

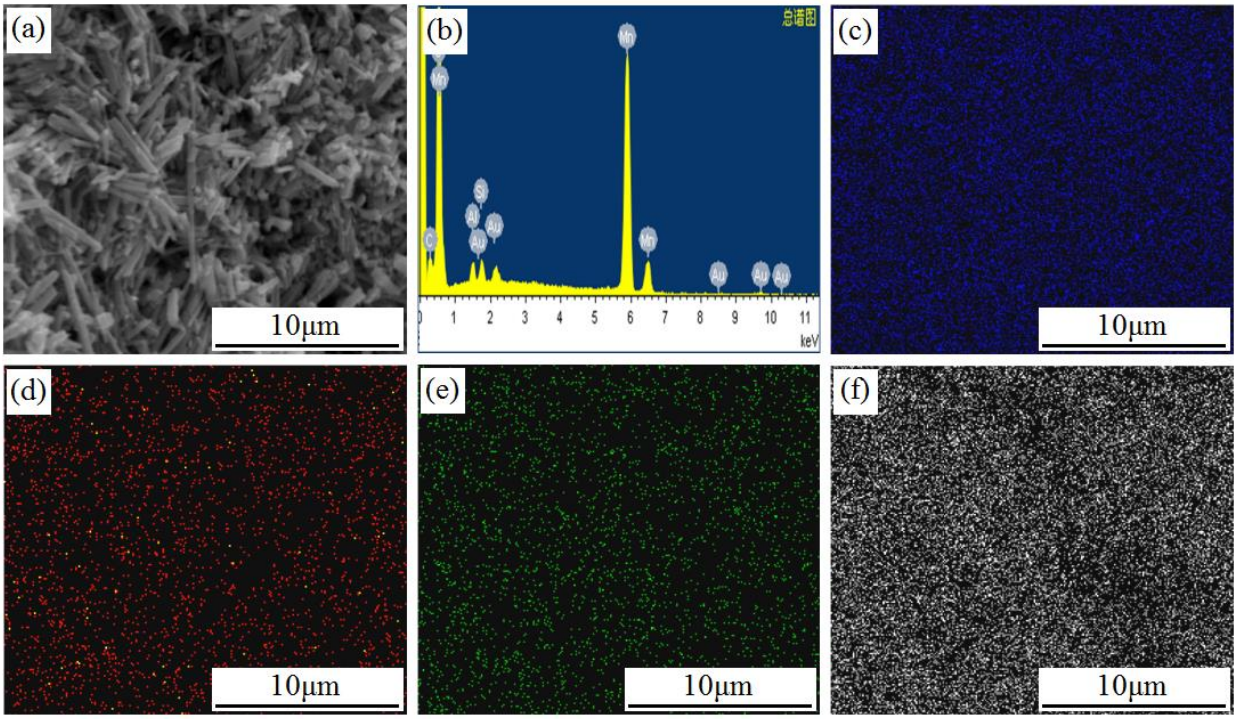

Figure 3. (a) SEM image, (b) EDS pattern and (d-f) Mapping images of the $LiMn_{1.92}Al_{0.04}Si_{0.04}O_4$ nanorods.

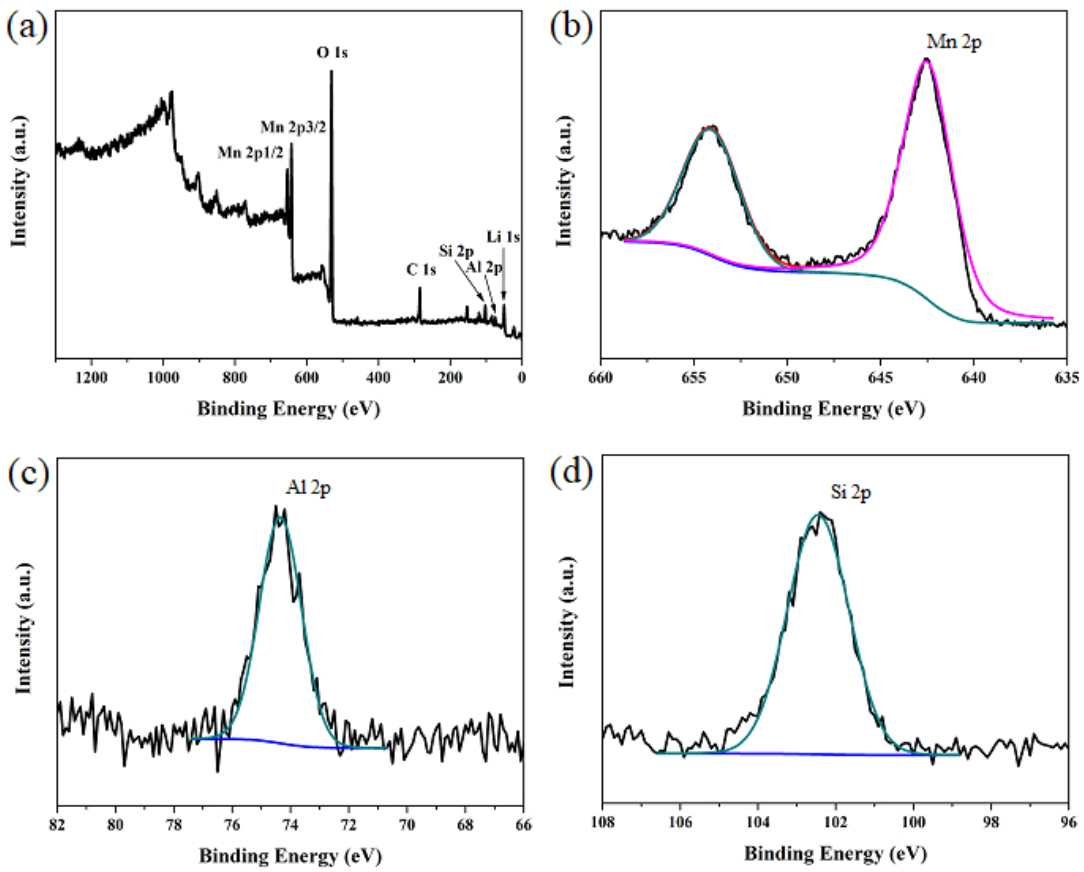

Figure 4. XPS spectra of the $LiMn_{1.92}Al_{0.04}Si_{0.04}O_4$ nanorods.

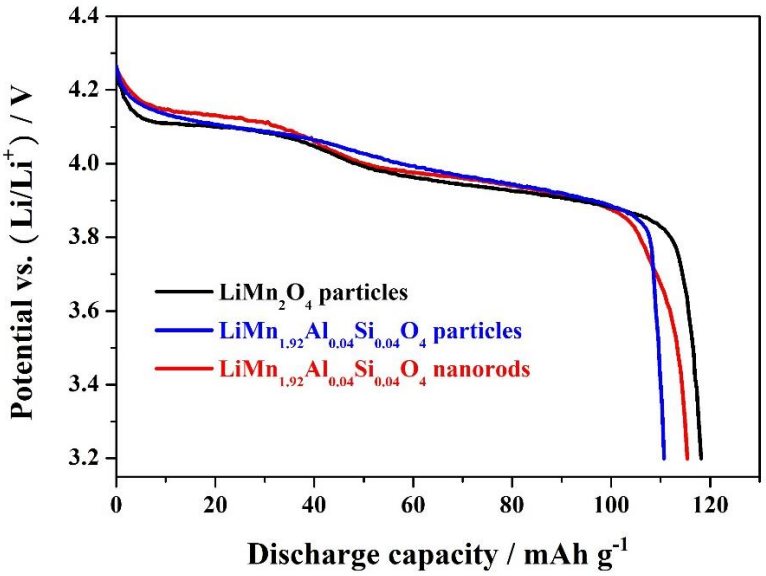

Figure 5. Initial discharge curves of the $LiMn_2O_4$ particles, $LiMn_{1.92}Al_{0.04}Si_{0.04}O_4$ particles and $LiMn_{1.92}Al_{0.04}Si_{0.04}O_4$ nanorods at 1.0 C.

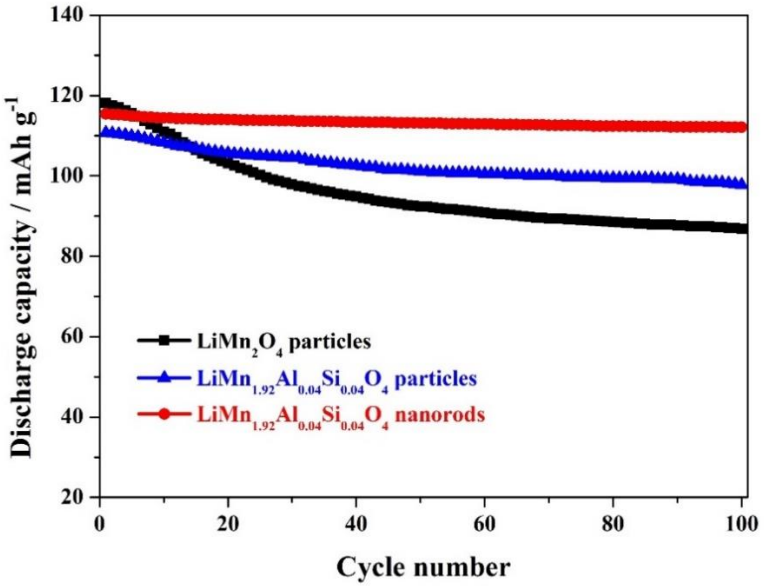

Figure 6. Cycling stability of the $LiMn_2O_4$ particles, $LiMn_{1.92}Al_{0.04}Si_{0.04}O_4$ particles and $LiMn_{1.92}Al_{0.04}Si_{0.04}O_4$ nanorods at 1.0 C.

Galvanostatic charge-discharge technology was employed to test the undoped $LiMn_2O_4$ particles, $LiMn_{1.92}Al_{0.04}Si_{0.04}O_4$ particles and $LiMn_{1.92}Al_{0.04}Si_{0.04}O_4$ nanorods so as to carry out investigation over the effect of both the Al-Si co-doping and nano-rod micrograph on the electrochemical performance of $LiMn_2O_4$. With these three samples cycled at 1.0 C, corresponding 1st discharge curves are shown in **Fig. 5.** Then, it can be observed that the characteristic voltage platforms of $LiMn_2O_4$ appear clearly in the discharge curves. In accordance with the result obtained from research [37, 38], it is evident that the intercalation/de-intercalation processes of lithium ions has close association with these two voltage platforms. It is of great importance to note that the voltage platform of the Al-Si co-doped $LiMn_2O_4$ samples has slight difference with that of the undoped $LiMn_2O_4$ particles at high voltage, which actually has close relationship with the addition of aluminum and silicon ions [24, 27].

Fig. 6 shows the cycling performance of the undoped $LiMn_2O_4$ particles, $LiMn_{1.92}Al_{0.04}Si_{0.04}O_4$ particles and $LiMn_{1.92}Al_{0.04}Si_{0.04}O_4$ nanorods. It can be shown that the undoped $LiMn_2O_4$ particles demonstrate a high reversible capacity of 118.2 mAh g^{-1} at 1.0 C and rather poor performance of cycling. In addition, corresponding capacity retention is only 73.5% after 100 cycles, which is mainly subject to the influence imposed by the distribution and agglomeration of non-uniform particle size [34]. The $LiMn_{1.92}Al_{0.04}Si_{0.04}O_4$ particles obtained can show better cycling stability with higher capacity retention in comparison with the undoped $LiMn_2O_4$ particles when the aluminum and silicon ions are added. Especially, the capacity retention for the $LiMn_{1.92}Al_{0.04}Si_{0.04}O_4$ nanorods reaches up to 97.1% after 100 cycles, which is much higher than that of the undoped $LiMn_2O_4$ particles, and the reversible capacity is a little greater than that of the $LiMn_{1.92}Al_{0.04}Si_{0.04}O_4$ particles. Furthermore, **Table 1** compares the cycling performance of both the $LiMn_{1.92}Al_{0.04}Si_{0.04}O_4$ nanorods and $LiMn_2O_4$-based cathode materials reported by other works [24,27,32]. According to the comparison result, it can be seen that the simultaneous use of the Al-Si co-doping and nano-rod micrograph plays an active role in enhancing the

cycling performance. It is then indicated by these results that the $LiMn_{1.92}Al_{0.04}Si_{0.04}O_4$ nanorods show excellent cycling performance, which mainly benefits from the positive effect imposed by doping with aluminum and silicon ions on inhibiting the Jahn-Teller distortion effect and strengthening the structural stability, as well as the promotion action of one-dimensional nanorod-like structure on the electron transport rate [27,32,39,40].

Table 1. Comparison of $LiMn_{1.92}Al_{0.04}Si_{0.04}O_4$ nanorods and $LiMn_2O_4$-based cathode materials reported by other works [24,27,32].

Sample	Cycling condition	Initial capacity (mAh g^{-1})	Capacity retention (%)
Al-doped $LiMn_2O_4$	5.0 C, 100 cycles	110.9	95[27]
Si-doped $LiMn_2O_4$	0.5 C, 100 cycles	134.6	85.1[24]
$LiMn_2O_4$ nanorods	1.0 C, 100 cycles	123.5	89.2[32]
$LiMn_{1.92}Al_{0.04}Si_{0.04}O_4$ nanorods	1.0 C, 100 cycles	115.4	97.1[This work]

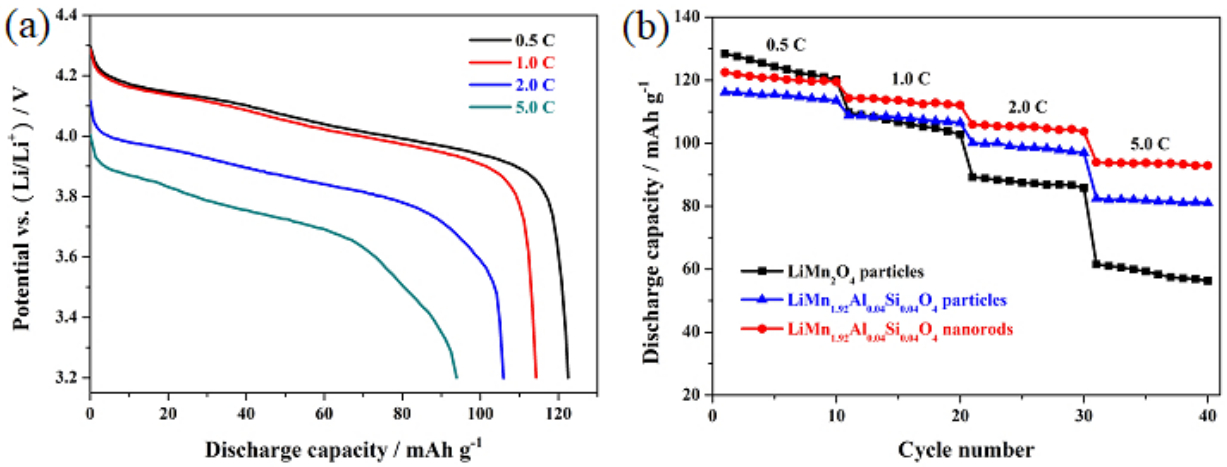

Figure 7. (a) Representative discharge curves of $LiMn_{1.92}Al_{0.04}Si_{0.04}O_4$ nanorods and (b) Rate capability of the $LiMn_2O_4$ particles, $LiMn_{1.92}Al_{0.04}Si_{0.04}O_4$ particles and $LiMn_{1.92}Al_{0.04}Si_{0.04}O_4$ nanorods.

Fig. 7a shows the representative discharge curves displaying the $LiMn_{1.92}Al_{0.04}Si_{0.04}O_4$ particles at different rates, and they are chosen mainly to represent these three samples. It can be observed from this figure that the high cycling rate has extremely great influence on the reversible capacity and voltage platform. It is shown that the values of these two indicators decreases gradually and the boundary between the two voltage platforms in discharge curve blurs gradually as the cycling rate increases, which has close relationship with the increased polarization. **Fig. 7b** displays the rate performance of these three samples at a variety of rates. It is quite obvious that the cycling rate is able to make a real difference to the reversible capacity. As for the undoped $LiMn_2O_4$ particles, the maximum reversible capacity obtained is 128.4 mAh g^{-1} at 0.5 C. More than that, the reversible capacity attenuates greatly as the cycling rate increases. When cycled at 5.0 C, this sample only delivers a low reversible capacity of 61.5

mAh g^{-1}, where the rather low retention is 47.9%. In sharp contrast, the samples of Al-Si co-doped $LiMn_2O_4$ can show excellent cycling stability at high rate. Especially, the reversible capacity of the $LiMn_{1.92}Al_{0.04}Si_{0.04}O_4$ nanorods maintains the value of 93.9 mAh g^{-1} at 5.0 C. It is then confirmed by such high performance that there is a synergetic effect of Al-Si co-doping and nano-sized rod-like micrograph on the rate capability of $LiMn_2O_4$.

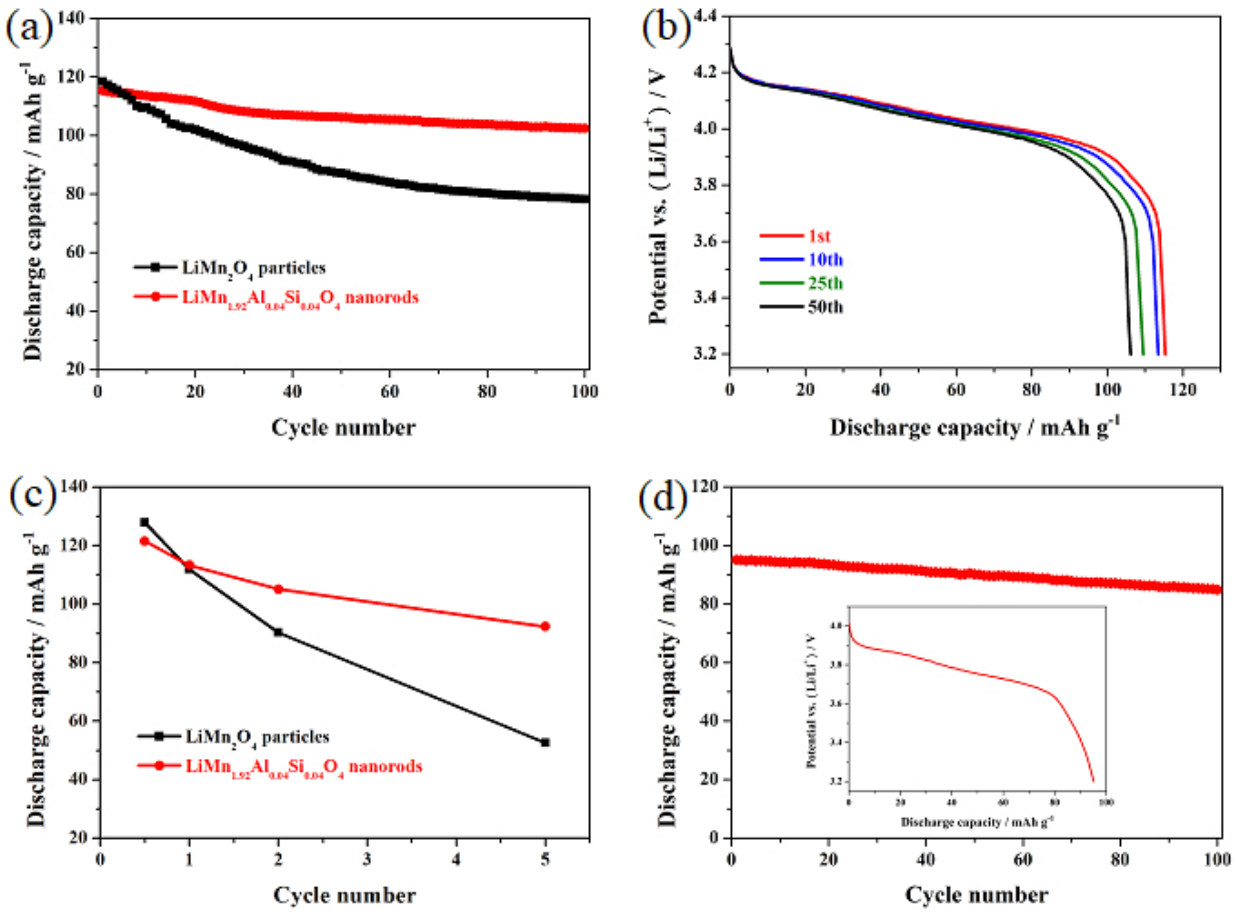

Figure 8. (a) Cycling stability of the $LiMn_2O_4$ particles and $LiMn_{1.92}Al_{0.04}Si_{0.04}O_4$ nanorods at 1.0 C under high temperature, (b) Representative discharge curves of the $LiMn_{1.92}Al_{0.04}Si_{0.04}O_4$ nanorods, (c) Rate capability of these two samples, and (d) Cycling stability of the $LiMn_{1.92}Al_{0.04}Si_{0.04}O_4$ nanorods at 5.0 C (Inset is the corresponding discharge curves).

The performance at high temperature is able to impose significant influence on the commercial application of $LiMn_2O_4$. **Fig. 8a** shows the performance at high temperature of the $LiMn_2O_4$ particles and $LiMn_{1.92}Al_{0.04}Si_{0.04}O_4$ nanorods at 1.0 C under the circumstance of high temperature (55 °C). It is shown that the undoped $LiMn_2O_4$ particles demonstrate pretty poor cycling stability. Despite the fact that the initial discharge capacity is comparable to the test results at room temperature, the capacity retention is far below the large-scale commercial application required for $LiMn_2O_4$. After 100 cycles, this sample only presents the capacity retention as low as 66.0% in spite of the decent initial capacity. In contrast, the $LiMn_{1.92}Al_{0.04}Si_{0.04}O_4$ nanorods can show an excellent capacity retention of 88.8% with satisfactory discharge capacity of 102.4 mAh g^{-1} after 100 cycles. **Fig. 8b** shows the representative

discharge curves of the $LiMn_{1.92}Al_{0.04}Si_{0.04}O_4$ nanorods, and it can be seen from the figure that the voltage platform shows no obvious change, which indicates the structural stability of the Al-Si co-doped $LiMn_2O_4$ nanorods.

Fig. 8c shows the rate capability of these two samples at the temperate of 55 °C. It can be observed that more stable high-temperature cycling stability for the $LiMn_{1.92}Al_{0.04}Si_{0.04}O_4$ nanorods are available at different rates, especially the high cycling rate. When cycled at 5.0 C, this sample can maintain the discharge capacity of 92.3 mAh g^{-1}, and it is 76.0% of the initial discharge capacity. In order to analyze the performance of high-rate cycling, the $LiMn_{1.92}Al_{0.04}Si_{0.04}O_4$ nanorods were cycled at 5.0 C. **Fig. 8d** shows that that the $LiMn_{1.92}Al_{0.04}Si_{0.04}O_4$ nanorods can deliver a satisfactory reversible capacity of 95.1 mAh g^{-1} and the capacity retention of 89.3% after 100 cycles at 5.0 C under high temperature. The results mentioned above confirm that the integration of Al-Si co-doping and nano-sized rod-like micrograph is able to result in obvious optimization effect on the performance at high temperature.

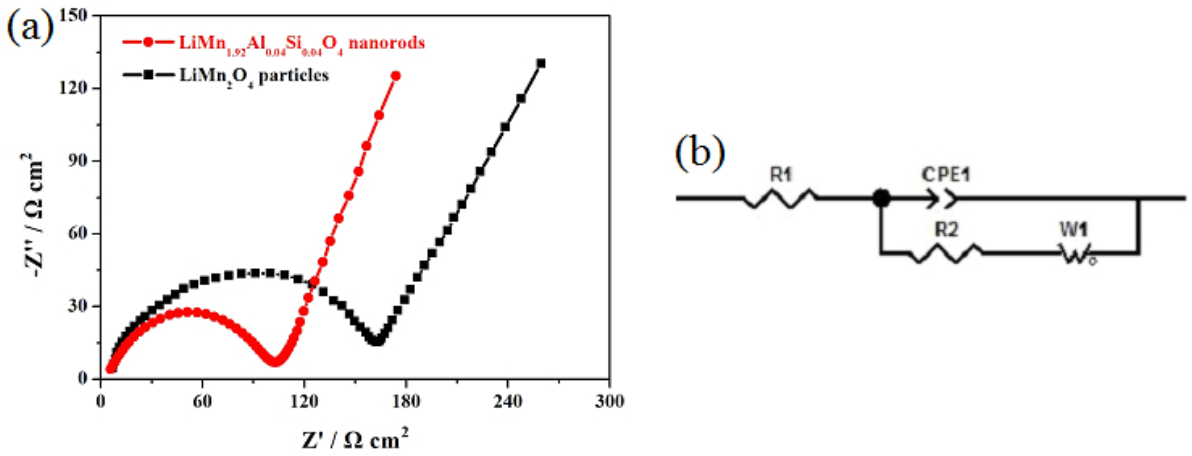

Figure 9. (a) Nyquist plots of the undoped $LiMn_2O_4$ particles and $LiMn_{1.92}Al_{0.04}Si_{0.04}O_4$ nanorods and (b) Equivalent circuit model of EIS.

Fig. 9a displays the Nyquist plots of the undoped $LiMn_2O_4$ particles and $LiMn_{1.92}Al_{0.04}Si_{0.04}O_4$ nanorods. It can be observed that the charge transfer resistance (R_2) is closely associated with the high-frequency region, which has close relationship with the electrochemical performance [9, 41, 42]. Therefore, the value of R_2 can be employed so as to study the effect of Al-Si co-doping and nano-sized rod-like micrograph on the electrochemical performance. **Figure 9b** shows the model of corresponding equivalent circuit. It can be found that the R_2 value is subject to the great influence of the Al-Si co-doping and nano-sized rod-like micrograph. Apart from that, the addition of aluminum ions and silicon ions is able to impose a positive effect on the reduction of the lithium-ion diffusivity [24, 41], and the one-dimensional nanorod-like structure is quite conducive to the improvement of electronic conductivity [42]. As far as the $LiMn_{1.92}Al_{0.04}Si_{0.04}O_4$ nanorods are concerned, the initial charge-transfer resistance is 92.7 Ω cm^2, which is less in comparison with that of the undoped $LiMn_2O_4$ particles. Actually, such

excellent result is mainly caused by the synergistic effect of Al-Si co-doping and nano-sized rod-like micrograph. In contrast, the undoped $LiMn_2O_4$ particles show higher value of R_2, which is always corresponding to the poor electrochemical performance. The results mentioned above indicate that the synergistic effect resulting from a combination of the Al-Si co-doping and nano-sized rod-like micrograph is of vital importance in enhancing the electrochemical performance of $LiMn_2O_4$.

4. CONCLUSIONS

To sum up, the electrochemical properties of $LiMn_2O_4$ are effectively improved through the comprehensive employment the Al-Si co-doping and nano-rod micrograph. The Al-Si co-doping fails to change the structure of $LiMn_2O_4$, and the rod-like micrograph of manganese source is inherited well from the Al-Si coped $LiMn_2O_4$ samples. It is the strategy of synergistic modification in this work that enables the best use of the inhibition of Al-doping on the Jahn-Teller distortion effect, the enhancement of Si-doping on the reversible capacity and the promotion of 1D nano-rod morphology on the electron transport rate. Since the synergistic effect is generated by the interaction between the Al-Si co-doping and nano-sized rod-like micrograph, the $LiMn_{1.92}Al_{0.04}Si_{0.04}O_4$ nanorods obtained are able to show more excellent electrochemical properties in comparison with the undoped $LiMn_2O_4$ and $LiMn_{1.92}Al_{0.04}Si_{0.04}O_4$ particles, which as a consequence can provide a valuable reference in promoting the commercial application of $LiMn_2O_4$.

ACKNOWLEDGMENTS
This work was financially supported by the Research Project of Science and Technology of Henan Province (No. 192102210301, No. 192102210215), Key Research Project of Education Department of Henan Province (No. 19A150023, No. 19A430014), Program for Innovative Research Team (in Science and Technology) in University of Henan Province (No. 20IRTSTHN016).

References

1. L. Li, Z. Li, A. Yoshimura, C. Sun, T. Wang, Y. Chen and S. F. Bartolucci, *Nat. Commun.,* 10 (2019) 1764.
2. Z. Liu, Q. Yu, Y. Zhao, R. He, M. Xu, S. Feng and L Mai, *Chem. Soc. Rev.,* 48 (2019) 285.
3. R. Li, W. Xiao, C. Miao, R. Fang, Z. Wang and M. Zhang, *Ceram. Int.,* 45 (2019) 13530.
4. Y. Cai, Y. Huang, X. Wang, D. Jia and X. Tang, *Ceram. Int.,* 40 (2014) 14039.
5. J. Deng, J. Pan, Q. Yao, Z. Wang, H. Zhou and G. Rao, *J. Power Sources,* 278 (2015) 370.
6. S. Huang, H. Wu, P. Chen, Y. Guo, B. Nie, B. Chen, H. Liu and Y. Zhang, *J. Mater. Chem., A,* 3 (2015) 3633.
7. L. Tian, C. Su, Y. Wang, B. Wen, W. Bai and J. Guo, *Vacuum,* 164 (2019) 153.
8. Y.L. Ding, J. Xie, G.S. Cao, T.J. Zhu, H.M. Yu and X.B. Zhao, *J. Phys. Chem., C,* 115 (2011) 9821.
9. J. Huang, F. Yang, Y. Guo, C. Peng, H. Bai, J. Peng and J. Guo, *Ceram. Int.,* 41 (2015) 9662.
10. Q. Wang, Y. Zhang, H. Zhang, Y. Xu, H. Dong and C. Zhao, *J. Alloys Compd.,* 693 (2017) 474.
11. X. Feng, J. Zhang and L. Yin, Powder Technol., 287 (2016) 77.
12. Y. Lu, X. Luo, H. Bai, J. Guo, M. Xiang, C. Su, X. Liu, W. Bai and R. Wang, *Vacuum,* 158 (2018) 223.
13. P. Chen, H. Wu, S. Huang and Y. Zhang, *Ceram. Int.,* 42 (2016) 10498.

14. X.H. Tan, H.Q. Liu, Y. Jiang, G.Y. Liu, Y.J. Guo, H.F. Wang, L.F. Sun and W.G. Chu, *J. Power Sources,* 328 (2016) 345.
15. D.-L. Fang, J.-C. Li, X. Liu, P.-F. Huang, T.-R. Xu, M.-C. Qian and C.-H. Zheng, *J. Alloys Compd.,* 640 (2015) 82.
16. D.-W. Han, W.-H. Ryu, W.-K. Kim, J.-Y. Eom and H.-S. Kwon, *J. Phys. Chem. C,* 117 (2013) 4913.
17. X. Feng, J. Zhang and L. Yin, Mate. Res. Bull., 74 (2016) 421.
18. H. Ming, Y. Yan, J. Ming, J. Adkins, X. Li, Q. Zhou and J. Zheng, *Electrochim. Acta,* 120 (2014) 390.
19. A. Tron, Y.D. Park and J. Mun, *J. Power Sources,* 325 (2016) 360.
20. R. Thirunakaran, T. Kim and W.-S. Yoon, *J. Sol-Gel Sci. Techn.,* 73 (2014) 62.
21. Z. Wang, J. Du, Z. Li and Z. Wu, *Ceram. Int.,* 40(2) (2014) 3527.
22. H.M. Wu, J.P. Tu, X.T. Chen, Y. Li, X.B. Zhao and G.S. Cao, *J. Solid State Electr.,* 11(2) (2005) 173.
23. W. Xu, Q. Li, J. Guo, H. Bai, C.-w. Su, R. Ruan and J. Peng, *Ceram. Int.,* 42 (2016) 5693.
24. H. Zhao, S. Liu, Z. Wang, Y. Cai, M. Tan and X. Liu, *Ceram. Int.,* 42(12) (2016) 13442.
25. S. Jayapal, R. Mariappan, S. Sundar and S. Piraman, *J. Electroanal. Chem.* 720-721 (2014) 58.
26. H. Zhao, F. Li, X. Bai, T. Wu, Z. Wang, Y. Li and J. Su, *Materials,* 11 (2018) 1302.
27. D. Guo, B. Li, Z. Chang, H. Tang, X. Xu, K. Chang, E. Shangguan, X.-Z. Yuan and H. Wang, *Electrochim. Acta,* 134 (2014) 338.
28. J.L. Wang, Z.H. Li, J. Yang, J.J. Tang, J.J. Yu, W.B. Nie, G.T. Lei and Q.Z. Xiao, *Electrochim. Acta,*75 (2012) 115.
29. A. Iturrondobeitia, A. Goñi, V. Palomares, I. Gil de Muro, L. Lezama and T. Rojo, *J. Power Sources,* 216 (2012) 482.
30. H. Jiang, Y. Fu, Y. Hu, C. Yan, L. Zhang, P.S. Lee and C. Li, *Small,* 10 (2014) 1096.
31. H.W. Lee, P. Muralidharan, R. Ruffo, C.M. Mari, Y. Cui and D.K. Kim, *Nano lett.,* 10(10) (2010) 3852.
32. H. Zhao, F. Li, X. Liu, W. Xiong, B. Chen, H. Shao, D. Que, Z. Zhang and Y. Wu, *Electrochim. Acta,* 166 (2015) 124.
33. H. Zhao, X. Liu, C. Cheng, Q. Li, Z. Zhang, Y. Wu, B. Chen and W. Xiong, *J. Power Sources,* 282 (2015) 118.
34. H. Zhao, S. Liu, Z. Wang, Y. Cai, M. Tan and X. Liu, *Electrochim. Acta,* 199 (2016) 18.
35. K. Chudzik, M. Lis, M. Świętosławski, M. Bakierska, M. Gajewska and M. Molenda, J. *Power Sources,* 434 (2019) 226725.
36. Q. Li, J. Zhang, C. Gong, J. Guo, L. Yu and J. Zhang, *Ceram. Int.,* 45 (2019) 13198.
37. L. Xiong, Y. Xu, T. Tao and J.B. Goodenough, *J. Power Sources,* 199 (2012) 214.
38. X. Xiao, J. Lu and Y. Li, *Nano Res.,* 3(10) (2010) 733.
39. X. Yi, X. Wang, B. Ju, Q. Wei, X. Yang, G. Zou, H. Shu and L. Hu, *J. Alloys Compd.,* 604 (2014) 50.
40. A. Iturrondobeitia, A. Goñi, L. Lezama, C. Kim, M. Doeff, J. Cabana and T. Rojo, *J. Mater. Chem. A,* 1 (2013) 10857.
41. Y. Duan, J. Guo, M. Xiang, J. Zhu, C. Su, H. Bai, X. Liu, W. Bai and R. Wang, *Solid State Ionics,* 326 (2018) 100.
42. H. Bai, W. Xu, J. Guo, C. Su, M. Xiang, X. Liu and R. Wang, *J. Mater. Sci.-Mater. El.,* 29 (2018) 14668.
43. M. Prabu, M.V. Reddy, S. Selvasekarapandian, G.V. Subba Rao and B.V.R. Chowdari, *Electrochim. Acta,* 88 (2013) 745.
44. Y.-L. Ding, J. Xie, G.-S. Cao, T.-J. Zhu, H.-M. Yu and X.-B. Zhao, *Adv. Funct. Mater.,* 21 (2011) 348.